Aerosol profiling with lidar in the Amazon Basin during the wet and dry season

H. Baars,[1] A. Ansmann,[1] D. Althausen,[1] R. Engelmann,[1] B. Heese,[1] D. Müller,[1,2] P. Artaxo,[3] M. Paixao,[1,3] T. Pauliquevis,[4] and R. Souza[5]

Received 21 June 2012; revised 24 August 2012; accepted 30 August 2012; published 3 November 2012.

[1] For the first time, multiwavelength polarization Raman lidar observations of optical and microphysical particle properties over the Amazon Basin are presented. The fully automated advanced Raman lidar was deployed 60 km north of Manaus, Brazil (2.5°S, 60°W) in the Amazon rain forest from January to November 2008. The measurements thus cover both the wet season (Dec–June) and the dry or burning season (July–Nov). Two cases studies of young and aged smoke plumes are discussed in terms of spectrally resolved optical properties (355, 532, and 1064 nm) and further lidar products such as particle effective radius and single-scattering albedo. These measurement examples confirm that biomass burning aerosols show a broad spectrum of optical, microphysical, and chemical properties. The statistical analysis of the entire measurement period revealed strong differences between the pristine wet and the polluted dry season. African smoke and dust advection frequently interrupt the pristine phases during the wet season. Compared to pristine wet season conditions, the particle scattering coefficients in the lowermost 2 km of the atmosphere were found to be enhanced, on average, by a factor of 4 during periods of African aerosol intrusion and by a factor of 6 during the dry (burning) season. Under pristine conditions, the particle extinction coefficients and optical depth for 532 nm wavelength were frequently as low as 10–30 Mm^{-1} and <0.05, respectively. During the dry season, biomass burning smoke plumes reached to 3–5 km height and caused a mean optical depth at 532 nm of 0.26. On average during that season, particle extinction coefficients (532 nm) were of the order of 100 Mm^{-1} in the main pollution layer (up to 2 km height). Ångström exponents were mainly between 1.0 and 1.5, and the majority of the observed lidar ratios were between 50–80 sr.

Citation: Baars, H., A. Ansmann, D. Althausen, R. Engelmann, B. Heese, D. Müller, P. Artaxo, M. Paixao, T. Pauliquevis, and R. Souza (2012), Aerosol profiling with lidar in the Amazon Basin during the wet and dry season, *J. Geophys. Res.*, *117*, D21201, doi:10.1029/2012JD018338.

1. Introduction

[2] The Amazon Basin is the largest hydrological basin in the world containing the largest extent of tropical rain forest on Earth – the Amazon rain forest. The tropical rain forest covers more than 5,000,000 square kilometers [*Nobre et al.*, 2004] and thus an area half as large as Europe or rather one third of South America. Because of its size and its pronounced hydrological cycle, the Amazon Basin is a key region for the global climate.

[3] From field campaigns during the last three decades (see review of *Martin et al.* [2010a]) it was concluded that Amazonia is at times very clean and free of anthropogenic influences in the wet season, while during the dry season smoke from vegetation fires heavily influences the atmospheric conditions. *Pöschl et al.* [2010] state that aerosol conditions in Amazonia's wet season "approach to those of the pristine pre-industrial era". Because of this strong contrast between the wet and the dry season, the Amazon Basin is considered to be favorable to study the direct and indirect aerosol effect on climate.

[4] Aerosol research in Amazonia was predominantly performed during the dry season with focus on biomass-burning aerosol (BBA) [*Kaufman et al.*, 1992; *Ward et al.*, 1992; *Kaufman et al.*, 1998; *Andreae et al.*, 2004]. During several field campaigns microphysical and optical properties of smoke aerosol were investigated mainly at the surface with in situ instrumentation [*Artaxo et al.*, 1994, 2002;

[1]Leibniz Institute for Tropospheric Research, Leipzig, Germany.
[2]Science Systems and Applications, Inc., NASA Langley Research Center, Hampton, Virginia, USA.
[3]Institute of Physics, University of São Paulo, São Paulo, Brazil.
[4]Department of Earth and Natural Sciences, Federal University of São Paulo at Diadema, Diadema, Brazil.
[5]University of the State of Amazonas, Manaus, Brazil.

Corresponding author: H. Baars, Leibniz Institute for Tropospheric Research, Permoserstr. 15, DE-04318 Leipzig, Germany. (baars@tropos.de)

0148-0227/12/2012JD018338

Guyon et al., 2003] and by means of airborne measurements [*Reid et al.*, 1998; *Reid and Hobbs*, 1998; *Chand et al.*, 2006]. Based on such BBA measurements, estimations of the direct aerosol effect were made [*Ross et al.*, 1998] and hypotheses were formulated concerning the aerosol semi-direct [*Koren et al.*, 2004] and indirect effect [*Reid et al.*, 1999; *Andreae et al.*, 2004; *Koren et al.*, 2004; *Rosenfeld et al.*, 2008]. However, most of these campaigns were performed in the southern cerrado regions and thus may not be representative for the entire Amazon Basin.

[5] Aerosol research in the wet season was less frequent and focused on natural aerosol from the rain forest. Biogenic aerosol (primary organic and secondary organic aerosol) from the forest was identified as the dominant aerosol species during that season [*Artaxo et al.*, 1988; *Martin et al.*, 2010b].

[6] Events of Saharan dust advection occasionally take place during the wet season and can significantly change the atmospheric aerosol conditions over the Amazon rain forest during that time [*Talbot et al.*, 1990; *Artaxo et al.*, 1990; *Swap et al.*, 1992; *Formenti et al.*, 2001; *Ben-Ami et al.*, 2010]. However, recently it was found that also BBA from African vegetation fires reaches the Amazon Basin together with Saharan dust and significantly disturbs the clean background conditions [*Kaufman et al.*, 2005; *Ansmann et al.*, 2009; *Baars et al.*, 2011]. BBA then frequently dominates the optical aerosol properties.

[7] As a consequence of the low natural aerosol concentrations, the impact of anthropogenic aerosol on rainfall production (aerosol indirect effect) may have a greater importance in the Amazon Basin than in other continental regimes [*Roberts et al.*, 2001; *Artaxo et al.*, 1990]. The knowledge of the vertical aerosol structures, and thus the information whether and in which way aerosols may alter cloud processes (liquid drop and ice particle formation) is essential to estimate the aerosol effects on climate. However, advanced aerosol measurements in the tropical Amazon rain forest are demanding and are constrained by the lack of infrastructure in this large inaccessible area. Long-term observations of the aerosol conditions in Amazonia have been performed by means of AERONET Sun photometer measurements [*Holben et al.*, 1996; *Schafer et al.*, 2008]. But to our knowledge no continuous measurements of vertical aerosol profiles have been performed before 2008.

[8] For the first time in Amazonia, continuous aerosol observations with Raman lidar were carried out in the framework of EUCAARI (European Integrated Project on Aerosol, Cloud, Climate, Air Quality Interactions) [*Kulmala et al.*, 2011] and AMAZE-08 (Amazonian Aerosol Characterization Experiment) [*Martin et al.*, 2010b]. Raman lidar is of unique advantage due to two reasons. Direct extinction profiling is performed at ambient humidity conditions (i.e., in the natural environment of aerosol layers) which is of fundamental importance for climate-impact studies. Second, the aerosol is remotely sensed and thus not manipulated before the measurement of optical and microphysical properties. In the case of surface-based or airborne in situ aerosol characterization the particles are dried and the full size distribution is not measured because of inlet and associated size cutoff effects. We have used the multiwavelength aerosol Raman lidar technique since 1997 and have performed several aerosol studies in polluted tropical areas in South Asia [*Franke et al.*, 2003] and West Africa [*Tesche et al.*, 2011]. In the framework of EUCAARI, Raman lidars were deployed in northern China close to Beijing [*Hänel et al.*, 2012], India [*Komppula et al.*, 2012], and South Africa.

[9] The paper is structured as follows: In section 2 the field site, the lidar instrument and the lidar data analysis methods are briefly described. Section 3 presents three case studies of particle optical properties, for aged smoke, young smoke, and pristine aerosol conditions observed during the wet season. Statistical results are given in section 4 in terms of layer geometrical properties describing the vertical extent of the aerosol layers and optical properties of aerosols. Statistical results for the wet and the dry season are contrasted. Concluding remarks and essential findings are summarized in section 5.

2. Experiment

2.1. Field Site

[10] The lidar observations were performed 60 km north of Manaus, which is on the Amazon river, at the Silvicultura research site of the National Institute for Amazonia Research (INPA). The field site at 2° 35.9′S, 60° 2.3′W and 83 m height above sea level (asl) in the central northern part of the Amazon Basin is indicated in Figure 1. The lidar was deployed on a glade surrounded by tropical rain forest which covers the sparely populated area upwind of the lidar site for almost 1000 km. Northeasterly (wet season) to easterly and southeasterly winds (dry season) prevail throughout the entire year as a result of the trade-wind circulation. The wet season lasts from December to June and the dry season from July to November. During the dry season, a high fire activity occurs in Amazonia each year. Due to the strong easterly trade winds, advection of pollution from the two-million-inhabitants city Manaus (the so-called Manaus plume) to the field site can generally be ignored [cf. also *Kuhn et al.*, 2010]. An AERONET (Aerosol Robotic Network) [*Holben et al.*, 2001] Sun photometer was mounted on a 15 m high tower at the lidar site. About 17 km west of the lidar location, the EUCAARI in situ measurements were performed using several research towers. Regular radiosondes are launched at the military airport of Manaus in the south of the city at 0000 UTC (2000 local time, LT) and 1200 UTC (0800 LT). In parallel to EUCAARI, the Amazonian Aerosol Characterization Experiment (AMAZE-08) [*Martin et al.*, 2010b] took place at the same sites in February and March 2008. Additional instruments for aerosol and gas investigations were operated during that time.

2.2. Lidar Instrument and Data Analysis

[11] The automated multiwavelength polarization Raman lidar Polly^{XT} (Portable Lidar System, XT indicates extended version) [*Althausen et al.*, 2009] was used for aerosol profiling. Observations were conducted from 22 January to 11 November 2008 and thus covered most of the wet and dry season. During the almost 10-months observational period, lidar observations could be performed on 211 days resulting in more than 2500 hours of tropospheric aerosol and cloud profile observations. Thus, a very high data coverage in terms of observation days could be achieved. A severe laser malfunction, however, interrupted the measurements in June/July for six weeks. For the rest of the observational

Figure 1. (left) Map of northern South America with lidar site (yellow star). The black line indicates the border of the rain forest. Source: http://earthobservatory.nasa.gov. (right) Satellite image of the experimental area showing the lidar site 60 km north of Manaus. Main wind direction from east is also indicated. Image source: Google Earth.

period, only minor interruptions due to, e.g., air-conditioning problems or power failures affected our observations.

[12] The advanced lidar permits us to measure vertical profiles of the particle backscatter coefficient at 355, 532, and 1064 nm, of the particle extinction coefficient at 355 and 532 nm, and of the particle depolarization ratio at 355 nm. From these extensive particle properties, intensive particle properties like the extinction-to-backscatter ratio (lidar ratio) and of the Ångström exponents can be calculated. The Ångström exponent expresses the wavelength dependence of the backscatter or extinction coefficient. Microphysical properties such as the effective radius, surface-area and volume concentrations, and the complex refractive index can be retrieved by means of an inversion scheme [*Müller et al.*, 1999a, 1999b; *Ansmann and Müller*, 2005]. The obtained volume size distribution and the complex refractive index allow us to estimate the single-scattering albedo (SSA) [*Müller et al.*, 2000]. Table 1 gives an overview of the aerosol products that can be derived from Polly^{XT} measurements.

[13] For the independent determination of particle backscatter and extinction coefficients, the Raman lidar method [*Ansmann et al.*, 1992] is applied. At daytime, when the Raman channels cannot be used, particle backscatter coefficients are retrieved with the Fernald algorithm [*Fernald*, 1984]. The volume and particle linear depolarization ratio are determined by following the method of *Murayama et al.* [1999]. Lidar signals are influenced by particle and Rayleigh backscatter and light-extinction processes. For the removal of Rayleigh scattering effects, molecular backscatter and extinction coefficients are computed after *Bucholtz* [1995] by using temperature and pressure profiles as measured with radiosonde launched at the Manaus military airport twice a day.

[14] More than 50 nighttime observations were available from the dry season measurements for extended aerosol profile studies using the Raman lidar technique. During the wet season, the prevalence of clouds, rain and fog made observing difficult. As a consequence, only the retrieval of the backscatter coefficients and the depolarization ratio was possible for most of the wet season measurements cases.

[15] Large uncertainties in the laser-beam receiver-field-of-view overlap correction in the lowest several hundreds of meters restrict the retrieval of the particle backscatter profiles to heights above about 400 m (Raman lidar method) or 750 m above ground level (agl) (Fernald method). Reliable particle extinction coefficients obtained with the Raman lidar method are available for heights above 1000 m after overlap correction by means of the method of *Wandinger and Ansmann* [2002]. The full overlap between the field of view of the telescope and the laser beam is achieved at 1500 m height. In summary, retrieval uncertainties are of the order of 5%–10% (backscatter coefficient, depolarization

Table 1. Overview of the Lidar-Derived Aerosol Products[a]

Parameter	Symbol	Remarks
Backscatter coefficient	β	355, 532, 1064 nm
Extinction coefficient	α	355, 532 nm
Linear depolarization ratio	δ	355 nm
Lidar ratio	$S = \frac{\alpha}{\beta}$	355, 532 nm
Ångström exponent	å	for α and β
Volume size distribution		via inversion
Effective radius	r_{eff}	via inversion
Number, surface, and volume concentration		via inversion
Complex refractive index		via inversion
Single-scattering albedo		inversion + Mie code

[a]An inversion scheme is used to derive microphysical properties and complex refractive index from the measured particle optical properties. Single-scattering albedo can be computed by means of a Mie scattering algorithm from the inversion products.

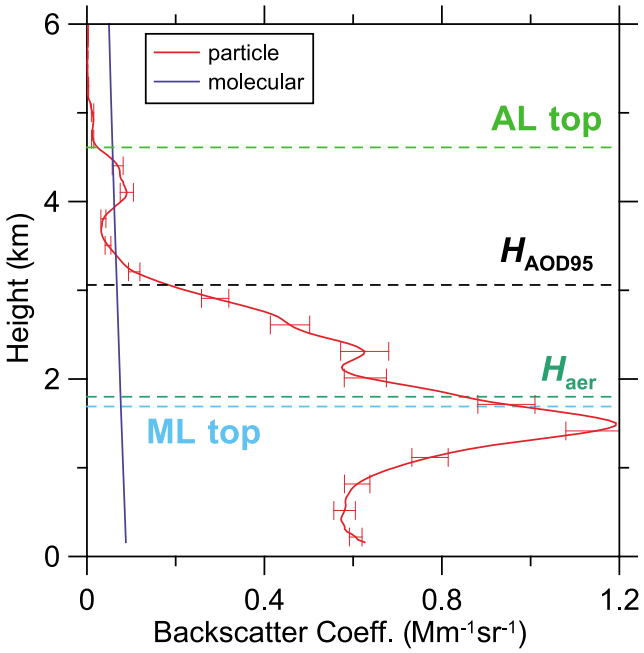

Figure 2. Four different layer height parameter used to characterize aerosol layering over the Amazon Basin. Aerosol layer height AL top, optical-depth-related scale height H_{aer}, H_{AOD95} (height at which 95% of the total AOD is reached), and ML top (top of the mixing layer as derived from ECMWF) are indicated as horizontal dashed lines. The vertical profile of the 1064 nm backscatter coefficient observed on 08 September 2008 is shown as measurement example (red curve with error bars).

ratio), 10%–20% (extinction coefficient), and 20%–30% (lidar ratio).

[16] The retrieval of the particle optical depth (AOD) was performed in the following way. When the profile of the particle extinction coefficient was available (dry season), these data were used in the AOD computation for the height range >1000 m. For heights <1000 m, the profile of the backscatter coefficient was taken. The particle backscatter coefficients were multiplied with the most appropriate lidar ratio, which is given by the Raman lidar observations of extinction and backscatter coefficient at heights in the upper part of the mixed layer (1–1.5 km height). For the lowermost 400 m for which no reliable backscatter coefficients are available, we assume height-independent backscattering and use the backscatter values for 400 m throughout the layer from the surface to 400 m height. This procedure leads to uncertainties in the AOD values of the order of 10% (during the dry season) as our sensitivity studies and comparisons with Sun photometer observations show. For the wet season measurements, the AOD retrieval is completely based on the backscatter coefficient profiles. A lidar ratio of 60 sr was generally assumed in the estimation of the particle extinction profile from the backscatter profile. The AOD uncertainty is then of the order of 25%–30% according to realistic variations in the lidar ratio from 40 to 80 sr.

[17] From the vertical profiles of the backscatter and extinction coefficients several geometrical parameter were derived, as illustrated in Figure 2. AL top is defined as the height, at which the 1064 nm particle backscatter coefficient drops below the threshold value of 0.02 Mm^{-1} sr^{-1} for the first time as a function of height. This threshold backscatter coefficient corresponds to a 1064 nm extinction coefficient of about 1 Mm^{-1} and a particle-to-Rayleigh extinction ratio of about 2 at 4 km height. H_{AOD95} is defined as that height at which 95% of the total AOD are caused by particles in the tropospheric layer below H_{AOD95}. The AOD scale height H_{aer} is defined as the height at which about 37% of the AOD ($1/e$ AOD) is caused by particles above H_{aer}. The mixing-layer top (ML top) is derived from European Centre for Medium-Range Weather Forecasts (ECMWF) model runs. These ML-top data are kindly provided by the Finnish Meteorological Institute.

[18] As a final remark, several efforts were undertaken to meet the hardware and software standards of the European Research Lidar Network (EARLINET) [*Pappalardo et al.*, 2010]. Calibration procedures were performed at the field site as well as afterwards at Leipzig, Germany, and applied, e.g., in the corrections of overlap effects and polarization effects in the receiver unit. These efforts as well as comparisons to other lidars and instruments (i.e., Sun photometer) showed that the measured aerosol profiles obtained with Polly^{XT} are of high quality and fulfill EARLINET standards [*Pappalardo et al.*, 2010, and references therein].

3. Case Studies

[19] Two cases with fresh (local) and aged smoke (regional haze) observed during the dry season are discussed in detail. They show very different optical and microphysical properties and thus provide an impression of the broad spectrum of smoke characteristics. As a contrast to the biomass burning cases, an observation at pristine conditions during the wet season with an AOD of less than 0.02 is presented in addition.

3.1. Aged Smoke

[20] *Reid et al.* [1998] provides a detailed explanation of the formation of aged biomass burning smoke in the Amazon Basin. After being emitted, the smoke particles disperse and have the potential to be rapidly transported into the lower atmosphere up to the strong trade wind inversion at a height of about 3–4 km as a result of the high air temperatures during emission. Smoke from hundreds of fires mix with biogenic emissions from forests and suspended soil particles (and potentially with urban haze). During transport, smoke undergoes photochemical transformations, gas-to-particle conversion, and particle coagulation. Smoke can be entrained into clouds where increased efficiencies of specific chemical reactions may accelerate the growth of the smoke particles.

[21] Based on their observations during SCAR-B (Smoke, Clouds and Radiation - Brazil), *Reid et al.* [1998] found that condensation and gas-to-particle conversion of inorganic and organic vapors increase the aerosol mass by 20%–45%. 30%–50% of this mass growth likely occurs in the first few hours. The remaining mass growth is probably associated with photochemical and cloud-processing mechanisms operating over several days. After three days, most of the condensation and gas-to-particle conversion has likely been taken place [*Reid et al.*, 1998]. Coagulation is then left to be

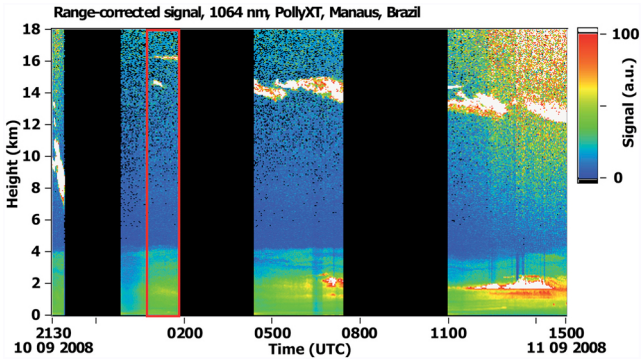

Figure 3. Aerosol layering observed from 10 September 2008, 2130 UTC (1930 LT) to 11 September 2008, 1500 UTC (1100 LT). The range-corrected signal at 1064 nm wavelength is shown. White features indicate low level clouds (around 2 km height agl) and ice clouds (mostly between 12 km height and the tropopause above 16 km height). The red box indicates the signal averaging period for an in-depth study of particle optical and microphysical properties.

the only significant particle growth mechanism over the next days of long-range transport.

[22] *Müller et al.* [2007a] investigated the growth of biomass burning particles as a function of travel time. They observed that the surface-area-weighted radius (effective radius) increases from values of 0.1 μm (1 day after emission), 0.15–0.25 μm (2–4 days after the emission) to values of 0.3–0.4 μm after 10–20 days of travel time. As shown by lidar observations [*Mattis et al.*, 2003] and subsequent model studies [*Damoah et al.*, 2004], fire smoke can survive over weeks in the free troposphere before it is removed by washout processes.

[23] The composition of the aerosol in the Amazon Basin can be divided into five possible components according to *Reid et al.* [1998]: primary smoke products, secondary smoke products, other anthropogenic materials, biogenic materials, and soils. The relative contribution of these components to the aerosol mass loading is highly variable. Continuously occurring changes in the particle size distributions and compositions during aging have a large impact on the optical properties of the aerosol. Different burning types (flaming and smoldering fires) increase the complexity of observed microphysical, chemical, and optical properties of smoke plumes.

[24] Our first case study deals with aged smoke. The lidar observations on 10 and 11 September 2008 are shown in Figure 3. A dense aerosol layer extended up to about 4 km. Cirrus occurred in addition, mainly in the upper troposphere. Fog (in the lowermost few hundred meters) occurred and prohibited high quality lidar observations from 0000–0030 UTC (2000–2030 local time, LT). Fog formation also attenuated the laser beam significantly between 0630 and 0700 UTC. The evolution of low clouds around 2 km height started after 0700 UTC on 11 September 2008.

[25] According to AERONET Sun photometer observations in the late afternoon on 10 September 2008 (2039 UTC), the total and fine-mode 500 nm AOD were 0.45 and 0.43 (fine-mode fraction of 95%). The 500 nm AOD increased to 0.6 in the morning of 11 September 2008 (1223 UTC). Photometer-derived Ångström exponents around 1.2 and effective radii of 0.23–0.26 μm on the late afternoon on 10 September 2008 are indicative for aged smoke [*Reid et al.*, 1998].

[26] Figure 4 (right) shows the 550 nm AOD over the Amazon Basin retrieved from MODIS (Moderate Resolution Imaging Spectroradiometer) [*Remer et al.*, 2005] observations on 10–11 September 2008. According to the satellite measurements, an aerosol plume was located southeast of the lidar site. AOD values up to 0.74 in southern Amazonia and of 0.5 for the Manaus region, respectively, were found.

[27] A very pronounced fire activity in the south, southeast, and east of the lidar site obviously caused this aerosol plume over Amazonia (see Figure 4, left). Fire counts for

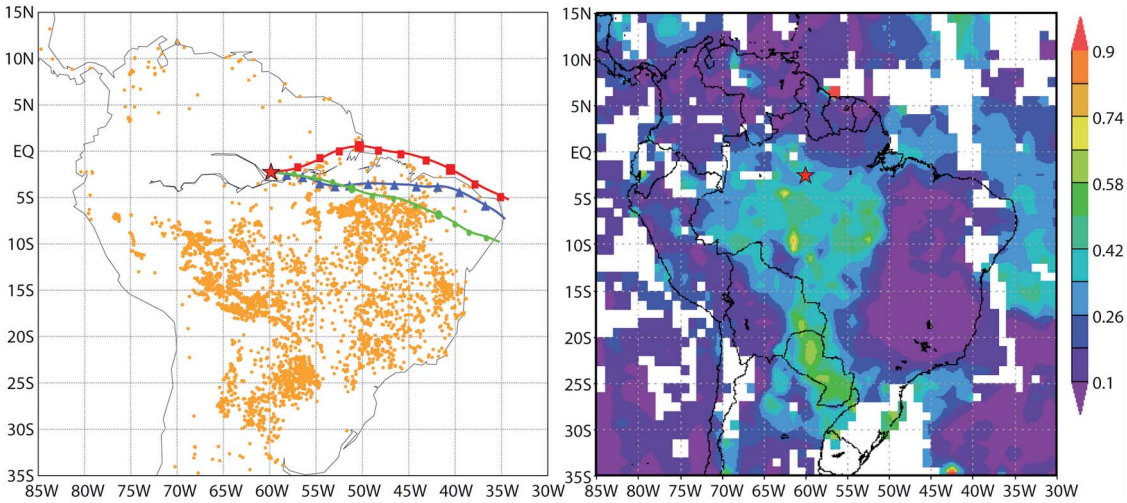

Figure 4. (left) Fire counts (orange dots) as derived by FIRMS for 7–10 September 2008 and HYSPLIT backward trajectories in 6-h steps (indicated by symbols) for the arrival heights of 1500 (blue), 3500 (red), and 5000 m agl (green) for 11 September 2008, 0100 UTC. (right) MODIS AQUA AOD composite (550 nm) for 10–11 September. The red star indicates the lidar site.

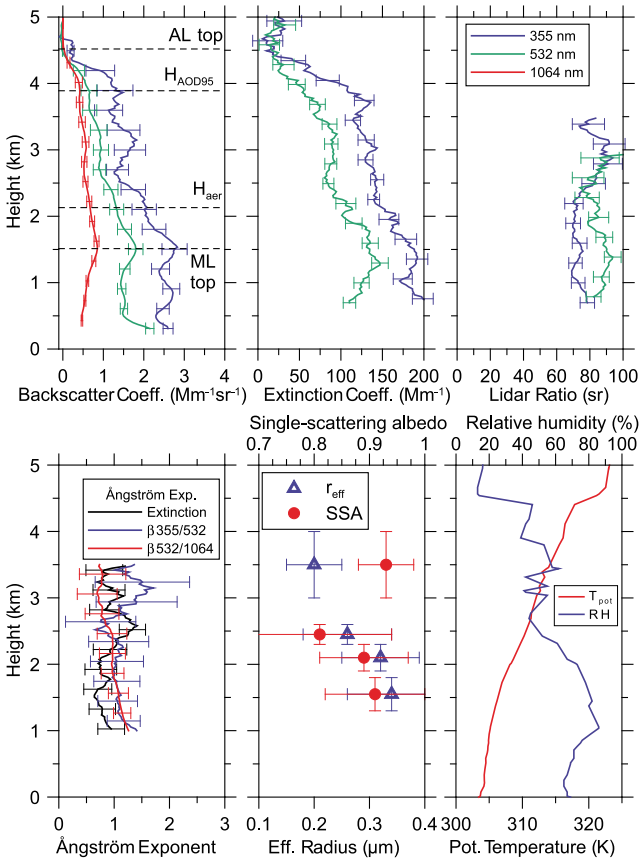

Figure 5. Vertical profiles of particle backscatter coefficient, extinction coefficient, and lidar ratio for several wavelengths, Ångström exponents, effective radius (r_{eff}), and single-scattering albedo (SSA) observed on 11 September 2008, 0100 UTC–0200 UTC (2100–2200 LT). The 532 nm AOD is 0.44. Potential temperature (T_{pot}) and relative-humidity (RH) profiles were measured with Manaus radiosonde launched on 11 September 2008, 0000 UTC. Different aerosol layer heights (AL top, H_{AOD95}, H_{aer}, ML top) are indicated by horizontal lines in the backscatter panel. Before the computation of the optical properties, lidar signals are vertically smoothed with window lengths of 270 m (backscatter), 750 m (extinction), and 990 m (lidar ratio). Layer mean values of effective radius and SSA are determined by inversion. Vertical bars indicate the layer depth.

7–10 September 2008 as obtained from MODIS measurements (via Fire Information for Resource Management System (FIRMS) at University of Maryland [*Giglio et al.*, 2003]) and 3-day backward trajectories for the arrival heights of 1500, 3500, and 5000 m from HYSPLIT (Hybrid Single Particle Lagrangian Integrated Trajectory Model, http://ready.arl.noaa.gov/HYSPLIT.php) are shown in Figure 4 [*Draxler and Hess*, 1998; *Draxler et al.*, 2009]. Meteorological fields from the archived model assimilation data sets of GDAS (NCEP Global Data Assimilation System) were used. The backward trajectories indicate an air-mass flow from easterly directions. The air masses crossed fire-active regions 1–2 days before the arrival at the lidar site. Freshly emitted smoke was added to the obviously already aged biomass burning aerosol (regional haze).

[28] The vertical profiles of the optical and microphysical properties of the smoke aerosol as observed with our lidar are presented in Figure 5 for the observation period between 0100 and 0200 UTC (indicated by a red box in Figure 3). Particle backscatter and extinction coefficients for the transmitted laser wavelengths, respective particle lidar ratios, Ångström exponents, effective radii, and SSA values (532 nm) determined for this one-hour period are shown. The vertical profiles of relative humidity and potential temperature derived from observations with radiosonde launched at the Manaus military airport at 11 September 2008, 0000 UTC, are given in addition.

[29] AL top height, H_{AOD95}, and the optical-depth-related scale height H_{aer} are 4.5, 3.9, and 2.1 km, respectively. The maximum mixing layer height ML top was about 1.6 km on 10 September 2008. AL top coincides with a strong temperature inversion (trade wind inversion layer). A moist atmosphere with relative humidities of 60%–80% within the lowermost 2.5 km of the troposphere, and 40%–50% from 2.5–4.5 km height was observed. 532 nm particle extinction coefficients were 150–200 Mm^{-1} for heights <2.5 km in the moist air, and 100–150 Mm^{-1} in the drier air. The similarity of the relative humidity and the extinction profiles indicate water uptake by the particles. The extinction coefficient for Amazonian smoke roughly increases by a factor of 1.5 when the relative humidity increases from 40% to 80% [*Rissler et al.*, 2006]. All in all, an almost vertically homogeneous haze layer was observed up to 4 km height. Ångström exponents are of the order of 1 and are thus in agreement with the Sun photometer observations.

[30] It is worth to mention that the observed particle depolarization ratio [*Baars et al.*, 2011] was always very low (<0.03) throughout the dry season. This observation corroborates the assumption that aged water-containing biomass burning particles can be regarded to be spherical.

[31] The lidar ratios of 70–90 sr shown in Figure 5 are indicative for considerably light-absorbing smoke particles [*Franke et al.*, 2003; *Müller et al.*, 2007b; *Tesche et al.*, 2011]. The larger lidar ratios at 532 nm compared to the ones for 355 nm in the main haze layer (below 2.5 km height) are another indication for the aged smoke (4–10 days old biomass burning particles) [*Müller et al.*, 2005; *Ansmann et al.*, 2009].

[32] The particle effective radius of about 0.3 μm in the main and humid aerosol layer below 2.5 km is roughly a factor of 2 larger than respective values found by *Reid et al.* [1998] for dry Amazonian smoke particles. Water uptake effects are responsible for these large effective radii on 11 September 2008. The effective radius decreases with height and is 0.2 μm in the drier air in upper part of the smoke layer.

[33] The lidar-derived SSA of the water-containing smoke particles of around 0.9 in the main layer below 2.5 km height are consistent with the values found by *Reid et al.* [1998] for dry smoke particles (0.8–0.9 for 550 nm) in southeastern Amazonia. The mass fraction of black carbon in the Amazonian smoke aerosol is in the range of 5%–10% [*Reid et al.*, 1998, 2005], but may vary from 2%–30% [*Reid and Hobbs*, 1998; *Reid et al.*, 2005]. *Tesche et al.* [2011] presented SSAs of, on average, even <0.8 (at 532 nm) for highly absorbing

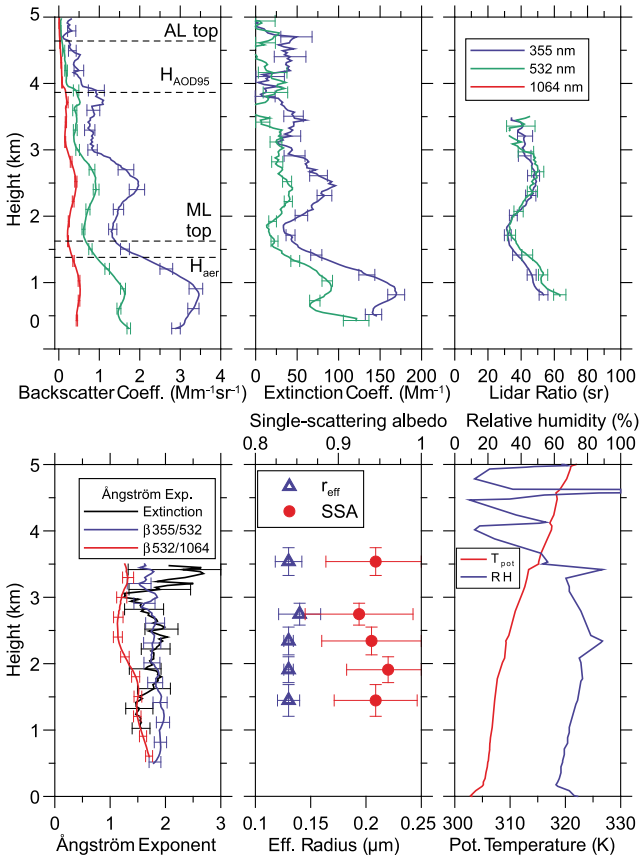

Figure 6. Same as Figure 5 except for 15 August 2008, 2235–2335 UTC (1835–1935 LT). AOD (532 nm) is 0.15. Potential temperature (T_{pot}) and relative humidity (RH) profiles were measured with Manaus radiosonde launched on 16 August 2008, 0000 UTC.

African smoke (at relative humidities below 60% in the smoke layers). *Dubovik et al.* [2002] reported AERONET-photometer-derived values from 0.9–0.94 for Amazon forest-fire smoke and 0.86–0.92 for South American savanna smoke (at ambient humidity conditions).

[34] In the drier layer between 3 and 4 km in Figure 5, the SSA slightly increased to values around 0.93. Different burning characteristics (smoldering versus flaming fires), differences in the burning material and thus composition of the smoke particles, and transport time may be responsible for the differences in the smoke optical properties, effective radius, and single-scattering albedo observed with the lidar above and below 2.5 km height.

[35] Finally, we estimated the mass-specific extinction coefficients and smoke mass concentrations based on combined photometer-lidar observations [*Ansmann et al.*, 2012]. In the retrieval, a density of the smoke particles of 1.35 g/cm^3 is assumed [*Reid and Hobbs*, 1998; *Reid et al.*, 2005]. The specific extinction coefficients are around 4 m^2/g (AERONET photometer, evening of 10 September 2008) and 3.5 m^2/g (lidar, moist layer below 2.5 km height) and 4.5 m^2/g (lidar, dry layer above 2.5 km height). With increasing water content (and thus decreasing particle density toward 1 g/cm^3) the mass-specific extinction coefficient increase (e.g., toward 6 instead of 4.5 m^2/g). Reid derived mass-specific extinction coefficients of 4 ± 1 m^2/g (at 550 nm) for dry Amazonian smoke particles. By using a specific extinction coefficient of 4 m^2/g we obtain particle mass concentrations of 30–40 μg/m^3 in the main part of the smoke haze layer below 2.5 km height, and a value around 15 μg/m^3 for the dry layer from 3–4 km height.

3.2. Young Smoke

[36] A case dominated by freshly emitted smoke was observed in early evening of 15 August 2008 (1835–1935 LT). Lidar profiles of optical and microphysical properties are shown in Figure 6. *Reid et al.* [1998] mentioned that smoke emissions in Brazil have a strong diurnal cycle. Fires are generally ignited in the late morning through late afternoon. Thus haze sampled in the early evening are most likely to contain a large fraction of young smoke.

[37] The optical properties show a distinct layering of particles. AL top was close to 4.5 km and the optical-depth scale height H_{aer} at about 1450 m, almost coinciding with the maximum ML top in the afternoon of 1600 m. 532 nm particle extinction coefficients ranged from 20–120 Mm^{-1} in the lowermost 3 km of the atmosphere. The 532 nm optical depth was 0.15. AERONET photometer observations are not available for this case because of persistent cirrus layers.

[38] The Ångström exponents were significantly higher than on 11 September 2008 (aged smoke case) with values of 1.5–2 for the wavelength range from 355–532 nm. Correspondingly, the effective radius was small with values around 0.13 μm. If we take the water-uptake effect into account (relative humidities ranged from 60–90% in the lowermost 3.5 km), the dry particle effective radius was certainly clearly below 0.1 μm. According to *Reid et al.* [1998], the high Ångström exponents of 1.5–2 and the very low effective radii point to freshly emitted smoke.

[39] The lidar ratios showed surprisingly low values for fresh smoke. We again expected highly absorbing particles and thus values >70 sr. The lidar ratio increases not only with increasing particle absorption but also with decreasing particle size. Such low values of 30–60 sr together with the high Ångström exponents indicate weakly absorbing particles. The negligible wavelength dependence of the lidar ratio is another characteristic for fresh smoke. The reason for these unusually low lidar ratios remains unclear. However, according to *Reid and Hobbs* [1998] and *Reid et al.* [2005], the black carbon content can vary from 2%–30%. *Müller et al.* [2005] presented statistics for Canadian and Siberian forest fire smoke (after travel times of >6 days) and also found lidar ratios spanning a large range from 30 to 90 sr. In agreement with the rather low lidar ratios, the SSA is high with values of 0.92–0.95 (see Figure 6, bottom).

[40] *O'Neill et al.* [2002] presents a Sun photometer study of aerosol properties at ambient conditions of boreal forest fires in western Canada. Several photometers were close to the fire sources (30–600 km), and others far way (>2000 km). For the small distances, the smoke-related fine-mode Ångström, effective radii, and single-scattering albedo, were 1.5–2.5, 0.13–0.17 μm, and mostly >0.95, respectively. For the large distances (aged smoke), they found lower Ångström exponents (1–1.5) and lower single scattering albedos (mostly <0.95). The effective radii were similar for the both data sets. These findings for boreal forest fires are

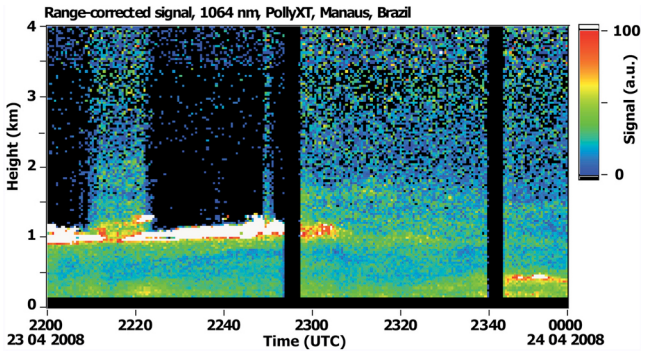

Figure 7. Temporal evolution of aerosol layering on 23 April 2008, 2200–2400 UTC (1800–2000 LT), in terms of the range-corrected 1064 nm signal. The mean 532 nm AOD for the 2300–0000 UTC period was estimated to be 0.019.

qualitatively in good agreement with our lidar observations of aged and young smoke.

3.3. Pristine Condition in the Wet Season

[41] The main results of the lidar observations performed during the wet season are discussed by *Baars et al.* [2011]. For the first time, clear and unambiguous indications for a significant long-range transport of African biomass burning aerosol to the Amazon Basin were documented [*Ansmann et al.*, 2009; *Baars et al.*, 2011].

[42] Here, we present one case obtained for rather pristine conditions to emphasize the strong contrast between natural aerosol conditions and man-made haze and smog situations in the Amazon Basin. Figure 7 shows the aerosol layering measured with lidar on 23 and 24 April 2008. Rain associated with strong washout effects was not observed during the complete lidar measurement session starting at 1800 UTC (1400 LT). In the beginning of the analyzed time period (at 2200 UTC), low-level clouds were present at around 1 km agl which prohibited the penetration of the laser beam to higher altitudes. At about 2300 UTC, the low-level clouds dissolved and the vertical extent of the aerosol layer of 2 km became visible to the lidar.

[43] The vertical profiles of the particle backscatter coefficient at 532 and 1064 nm and the respective Ångström exponent for the cloud-free period after 2330 UTC are shown in Figure 8. One aerosol layer near to the surface and a second aerosol layer centered at around 1 km height were observed. In the higher layer the low level clouds occurred. The particle backscatter coefficients multiplied with a lidar ratio of 60 ± 20 sr provide estimates for the 532 nm extinction coefficients. Values of 5–15 Mm^{-1} are rather low and indicate pristine conditions. The 532 nm AOD of 0.019 ± 0.008 was estimated from the extinction profile. The Ångström exponents of around 1.5 are typical for accumulation mode particles. Because of instrumental problems, no information from the UV channels was available on that day.

[44] The AOD of 0.019 is lower than the average AOD over clean marine sites [*Smirnov et al.*, 2009], and is one of the lowest values ever measured over a continental site. Measurements near Antarctica showed similar low AOD values [*Holben et al.*, 2001; *Wilson and Forgan*, 2002].

[45] The maximum ML top on that day was calculated to be 760 m. Thus, it was slightly higher than the observed top of the first aerosol layer. The AOD scale height H_{aer} was 960 m. The AL top and the height H_{AOD95} coincide at 1750 m.

[46] The low observed AOD value is even more remarkable when taking the high relative humidity of >80%–90% into account. Natural Amazonian aerosol was classified as moderately hygroscopic in previous experiments [*Zhou et al.*, 2002; *Rissler et al.*, 2004] so that hygroscopic growth should enhance the aerosol light scattering. In summary, one can conclude that the observed aerosol conditions on 23 April 2008 with an AOD of 0.02 represent background or natural aerosol conditions over the Amazon rain forest.

[47] Such pristine conditions with an AOD < 0.05 at 532 nm were observed in about 50% out of all measurement cases during the wet season. Aerosol was then trapped in the lowermost 2.5 km of the troposphere. However, in about one third of all measurements advection of smoke and dust aerosol from Africa was observed as discussed by *Baars et al.* [2011]. AODs ranged then typically from 0.07–0.25.

4. Statistical Results: Seasonal Aerosol Characteristics

[48] In this section, the essential results of the statistical analysis of the lidar measurements in the dry and wet season 2008 are presented and discussed. The general wind patterns prevailing in 2008 are analyzed in section 4.1. The geometrical properties are given in section 4.2. The statistical findings for the particle optical properties (backscatter and extinction coefficients, lidar ratio, Angström exponents, particle optical depth) are then discussed in section 4.3.

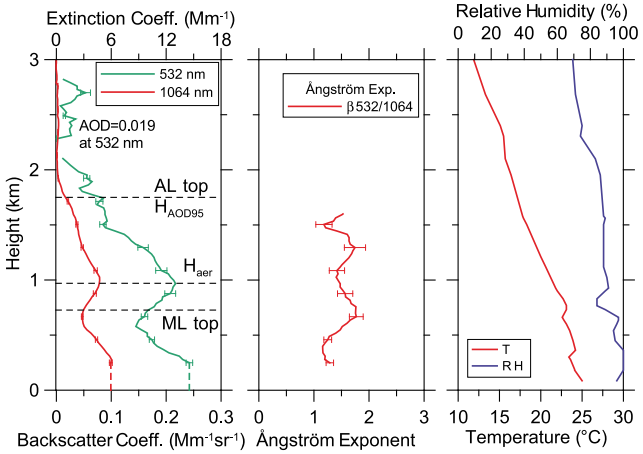

Figure 8. Vertical profiles of the 532 nm (green) and 1064 nm particle backscatter coefficient (red) and corresponding Ångström exponent measured on 23 April 2008, 2330–0000 UTC (1930–2000 LT). Extinction coefficient values (upper scale in the left panel) are obtained by multiplying the backscatter coefficient with a lidar ratio of 60 sr. The 532 nm AOD is estimated from the backscatter profile to be 0.019. Temperature (T) and relative humidity (RH) profile were measured with Manaus radiosonde on 24 April 2008, 0000 UTC. Different layer heights are indicated by horizontal lines in left panel.

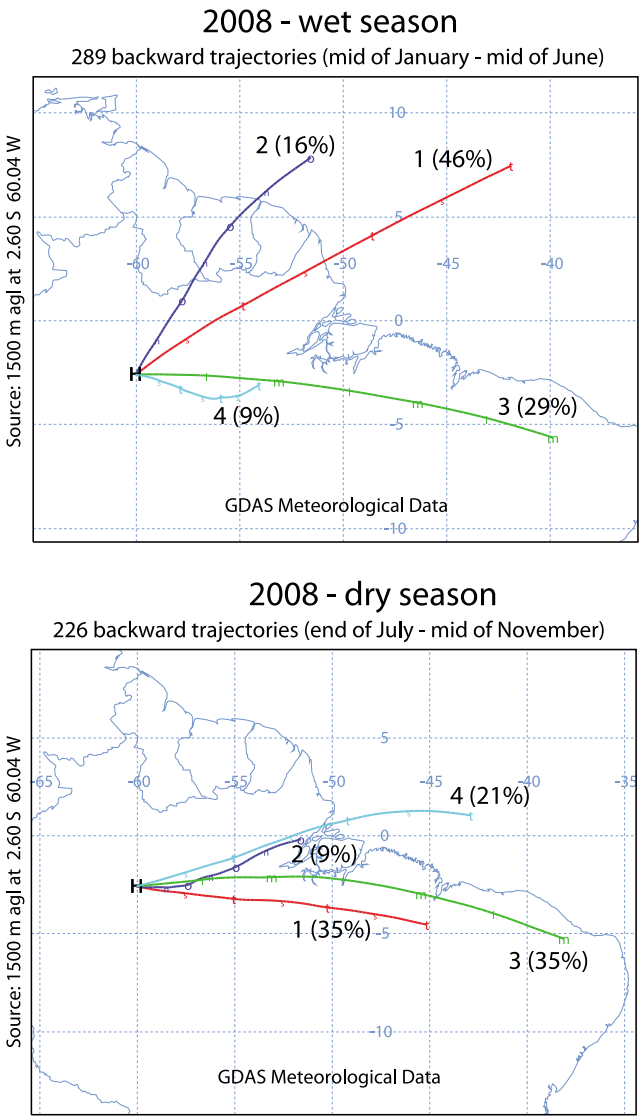

Figure 9. Cluster analysis of backward trajectories for the wet and dry season based on daily 172-h backward trajectories at an arrival height of 1500 m agl. Four clusters for each season were identified. The frequency of occurrence of each of the clusters (1–4) is given in brackets. Two trajectories per day (for arrival times of 0000 and 1200 UTC) were calculated.

4.1. Meteorological Conditions

[49] A cluster analysis (offline-version of HYSPLIT, version 4.9, http://ready.arl.noaa.gov/HYSPLIT.php) based on HYSPLIT backward trajectories for Manaus arrival height of 1500 m agl and arrival times of 0000 and 1200 UTC for each day from mid January to mid June 2008 (wet season) and from end of July to mid November 2008 (main part of the dry season) was performed. As shown in Figure 9, the analysis revealed that air masses were transported from easterly directions to the field site during both seasons as a result of the prevailing trade-wind circulation. Four clusters for each season were identified. In the wet season, mostly north-easterly air flows occur (in 62% out of all cases), whereas the air masses came mainly from easterly to south-easterly direction in the dry season (in 70% out of all cases).

[50] The backward-trajectory analysis also suggests that the impact of the Manaus pollution plume on the aerosol conditions at the field site was rare. These findings corroborate the results presented by *Kuhn et al.* [2010]. The authors showed that the Manaus pollution plume is usually transported to southwesterly directions. The dispersion of the Manaus plume was found to be low so that only regions directly downwind of the city were affected.

4.2. Layer Geometrical Characteristics

[51] Figure 10 shows histograms for the aerosol layer top height (AL top) and the AOD scale height (H_{aer}) separately for the wet and dry season. As can be seen, the top heights accumulated between 2 and 3 km during the wet season 2008. A broad distribution was found for the dry season with most values in the range from 3–5 km height. AOD scale heights H_{aer} were not very different during the wet and dry season. The main aerosol layer (below H_{aer}) reached to 500–1500 m (wet season) and 1000–2000 m (dry season) most of the time.

[52] Figure 11 shows time series of AL top, H_{aer}, and H_{AOD95} in 2008. In terms of the different layer depths a pronounced shift toward higher values and larger spread of the layer depths during the dry season is visible. However, H_{aer} shows less variability than the AL top height. Mean values of AL top, H_{AOD95}, H_{aer}, and ML top are 4.1, 3.0, 1.6, and 1.5 km for the dry season, and 2.5, 2.3, 1.2, and 1.1 km for the wet season. The AOD scale height almost coincides with mixing layer height during both seasons. The depth of the layer which causes 95% of the AOD was almost the same as the aerosol top height during the wet season, but was often considerably below the height at which the last traces of particles are detected during the dry season. On average, AL top in the dry season was 1.5 km higher than in the wet season whereas the main contribution to the particle optical depth stems from the particle below about 1.5 km disregarding the season.

4.3. Particle Optical Properties

4.3.1. Backscatter Profiling

[53] Figure 12 shows mean profiles of the 532 nm particle backscatter coefficient for pristine conditions during the wet season, for periods with advection of African dust and smoke during the wet season, and for the dry season. Cloud-screened observations are considered only. All individual one or two-hour mean backscatter profiles observed on more than 50 different days during the dry season are shown to indicate the strong variability of the optical properties as a function of burning intensities, atmospheric layering conditions, and varying relative humidity conditions. Throughout the entire dry and wet seasons, aerosol layers above 6.5 km were not detected. Compared to pristine condition in the wet season, the backscatter coefficients are, on average, enhanced by a factor of 6. However, during events with African aerosols, the particle backscatter level is also clearly larger (by a factor of 4) compared to undisturbed Amazonian aerosol conditions [*Baars et al.*, 2011].

[54] Histograms of the backscatter-related Ångström exponents in the dry season (Figure 13) peak at values

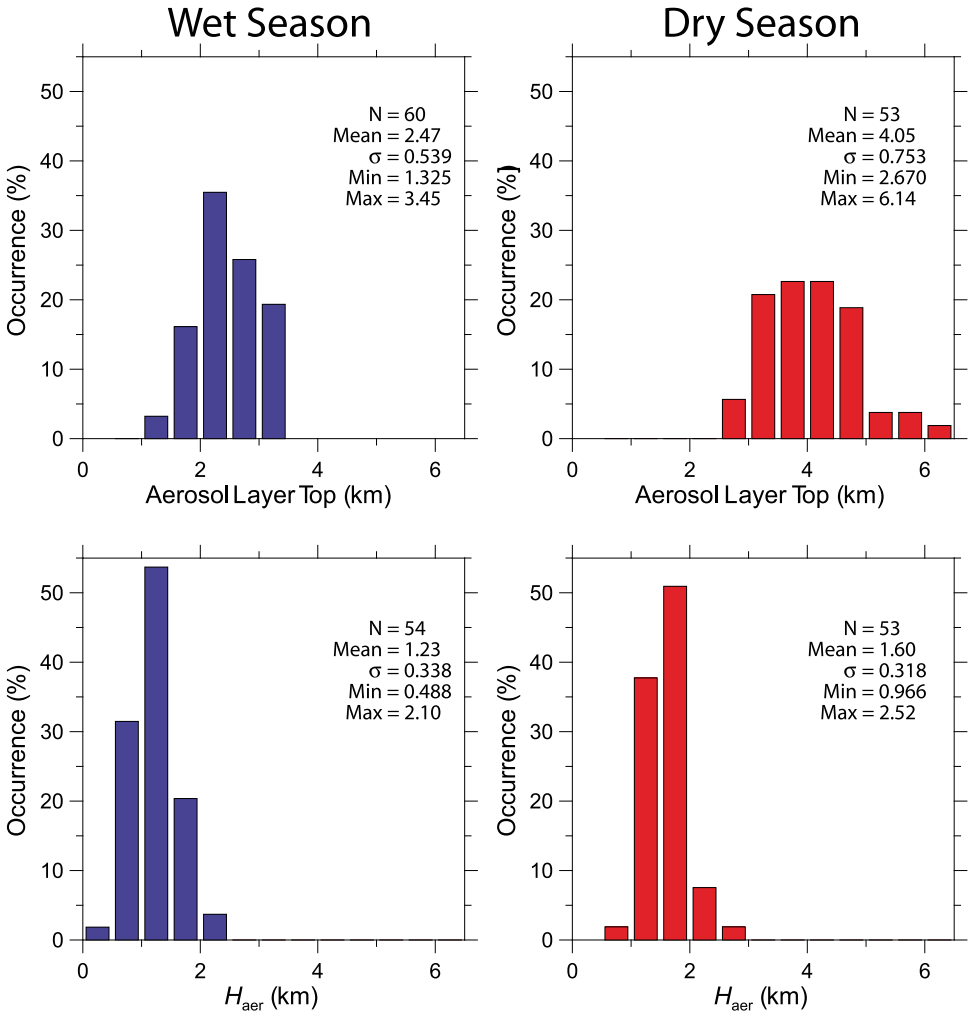

Figure 10. Frequency distribution of (top) AL top and (bottom) optical-depth-related scale height H_{aer} for the wet season (blue) and the dry season (red). The statistics are based on N observations. Mean values, standard deviations, maximum and minimum values are given as numbers.

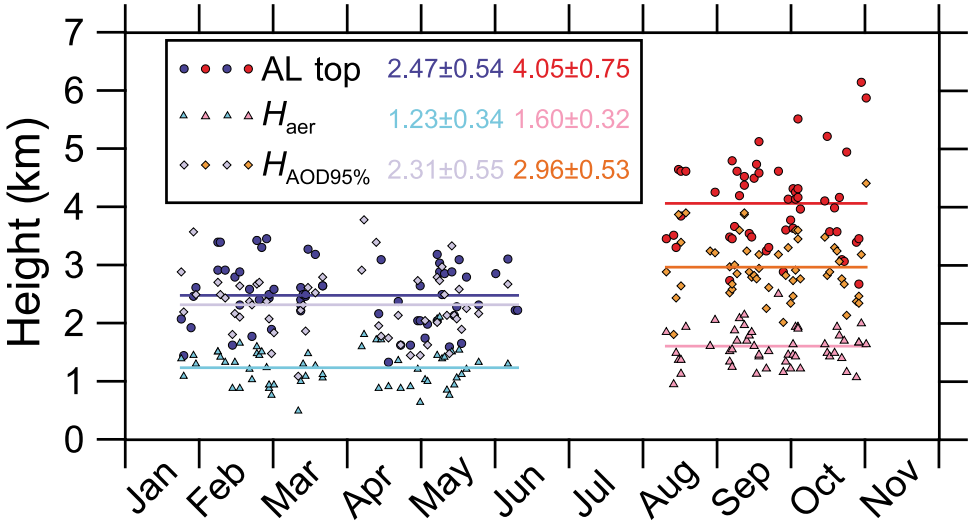

Figure 11. Time series of AL top, H_{AOD95}, and H_{aer} for the wet (blue colors) and dry season (red colors) in 2008. Horizontal lines indicate the mean values (given also as numbers).

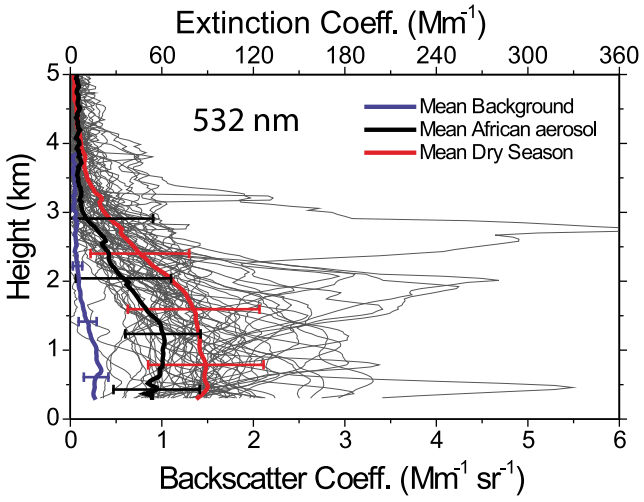

Figure 12. Mean profiles (thick solid lines) with standard deviations (thick bars, indicating the atmospheric variability) of the 532 nm particle backscatter coefficient for background conditions in the wet season (blue), conditions with African aerosol advection during the wet season (black), and as observed during the dry season (red). All individual profiles (thin grey lines) measured during the dry season are shown in addition to illustrate the strong variability and vertical inhomogeneity of smoke contamination during the burning season. Extinction scale (upper axis) is simply given by multiplying the backscatter scale with a lidar ratio of 60 sr.

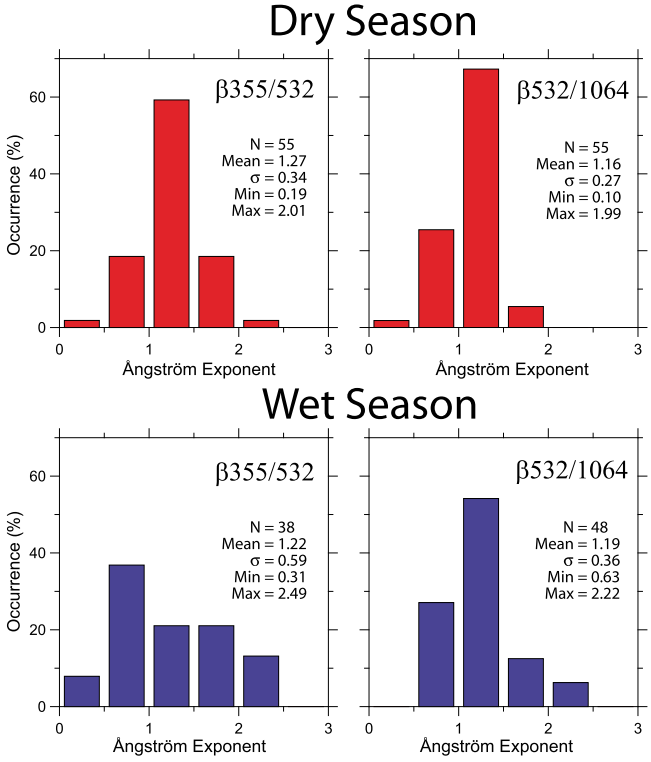

Figure 13. Frequency distributions of backscatter-related Ångström exponents for the two different spectral ranges from 355–532 and 532–1064 nm. The histograms are based on *N* layer mean values (1500–2500 m height range) for the dry (red) and wet (blue) season. Mean values, standard deviations, and maximum and minimum values are given as numbers.

between 1–1.5 for both, the short-wavelength and the long-wavelength range, which may be interpreted as a clear indication for the dominance of a well pronounced accumulation size mode of aged smoke particles. Similar distributions were observed for aged Asian particles over the tropical Indian Ocean [*Franke et al.*, 2003] and for African smoke [*Tesche et al.*, 2011]. For the wet season, the broad Ångström exponent spectrum (Figure 13) for the 355–532 nm spectral range indicates less well defined aerosol conditions as a consequence of the occurrence of local aerosols (of biogenic origin with a small content of marine particles) as well as of African aerosols with variable fractions of dust and smoke.

4.3.2. Extinction Profiling

[55] Figure 14 shows the seasonal mean profile of the 532 nm particle extinction profile for the dry season together with the individual profiles for more than 50 nights. These profiles are directly derived from the nitrogen Raman signals after cloud-screening. The profile of the corresponding mean Ångström exponent in Figure 14 is computed from the individual profiles of the Ångström exponent, which in turn are calculated by using the individual observations of the 355 and 532 nm extinction profiles. A strong variability of the extinction values is found. Compared to the backscatter coefficients, which can be determined with high vertical resolution of 60–300 m, the Raman signal profiles are smoothed for the retrieval of the extinction coefficients with a vertical window length of 750 m. For this reason, the vertical variability of the extinction coefficient is reduced compared to the backscatter variability in Figure 12. On average during the dry season, 532 nm extinction values are mostly found

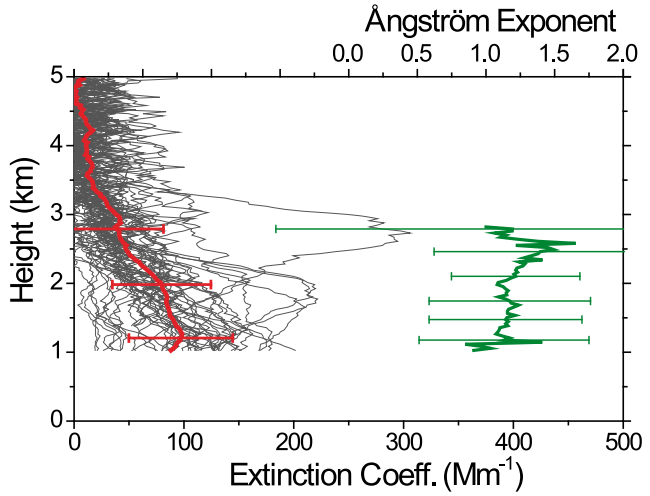

Figure 14. Mean profiles (thick solid lines) with standard deviations (thick bars, indicating the atmospheric variability) of the 532 nm particle extinction coefficient (red) and the Ångström exponent (green, 355–532 nm spectral range). These data are derived by applying the Raman lidar technique to the dry season observations. All individual extinction profiles measured during the dry season are shown in addition in grey to illustrate the variability and vertical inhomogeneity of smoke contamination.

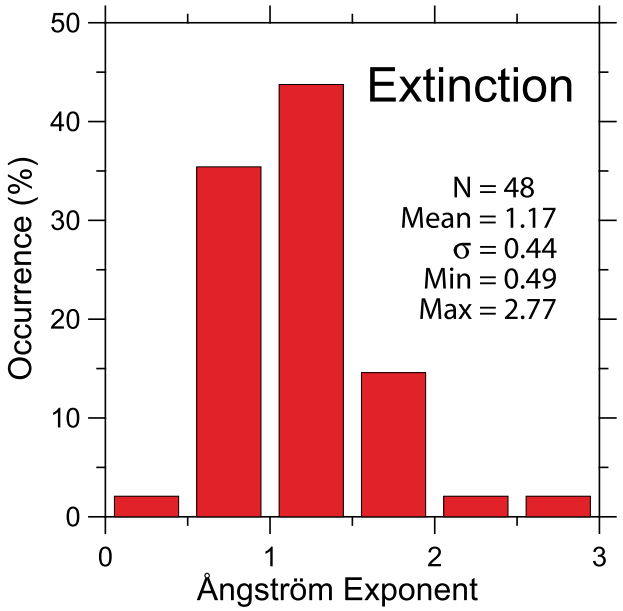

Figure 15. Frequency distributions of layer mean extinction-related Ångström exponent derived from *N* observations in the dry season. Mean values for layer from 1500–2500 m agl are considered. The statistics are based on *N* observations. Mean values, standard deviations, maximum and minimum values are given as numbers.

around 100 Mm^{-1} in the lowermost 2 km of the moist atmosphere over the Amazon rain forest close to Manaus.

[56] As mentioned, wet-season extinction profiles data (by using the Raman lidar method) can not be presented because of the high frequency of low-level clouds, rain, and fog. These unfavorable conditions prohibited temporal averaging of the lidar signal for more than one hour which is necessary for the determination of the extinction coefficient profile with Polly^{XT} under very clean conditions.

[57] The mean profile of the extinction-related Ångström exponent in Figure 14 is in agreement with the backscatter-related Ångström values in Figure 13. On average, the values range from 1–1.5 throughout the aerosol column. The frequency distribution of the extinction-related Ångström exponents found during the dry season is shown in Figure 15. Frequently occurring values from 0.5–1.5 indicate comparably large particles. The size of the particles may be widely controlled by hygroscopic growth and growth during long-range transport by condensation of gases and by coagulation.

[58] Similar Ångström exponent values were observed by *Schafer et al.* [2008] for the northern Amazon rain forest regions from AERONET observations. In the southern forest and cerrado regions, however, the authors report a frequent occurrence of Ångström exponent >1.5 during the dry season. *Guyon et al.* [2003] even reported Ångström exponents above 2 over Alta Floresta in southern Amazonia. The extinction-related Ångström values are in good agreement with respective values found from Raman lidar observations of aged biomass-burning plumes during the dry season in southern, tropical Asia [*Franke et al.*, 2003] and during the dry season in western Africa [*Tesche et al.*, 2011].

4.3.3. Extinction-to-Backscatter Ratio

[59] Figure 16 shows the lidar ratio (extinction-to-backscatter ratio) statistics for the dry season 2008. Mean values for the central part of the smoke plumes (1500–2500 m height) were analyzed. Lidar ratios ranged from 25 and 95 sr. The predominance of the lidar ratios were between 50 and 70 sr (in 61% out of all cases) for 355 nm and 50 and 80 sr (in 71% of all cases) for 532 nm. Together with the fact that the Ångström exponents indicate, on average, relatively large particle theses high values indicate moderately to strongly absorbing particles. For given chemical properties, the lidar ratio decreases with increasing particle size and decreasing absorption efficiency of the particle ensemble [*Müller et al.*, 2007a]. In about 42% out of the cases, the lidar ratios at 532 nm exceeded 70 sr which is clear sign for strongly absorbing smoke particles. Such high values were found for African smoke [*Tesche et al.*, 2011] and southern Asian smoke [*Franke et al.*, 2003] originating from northern India.

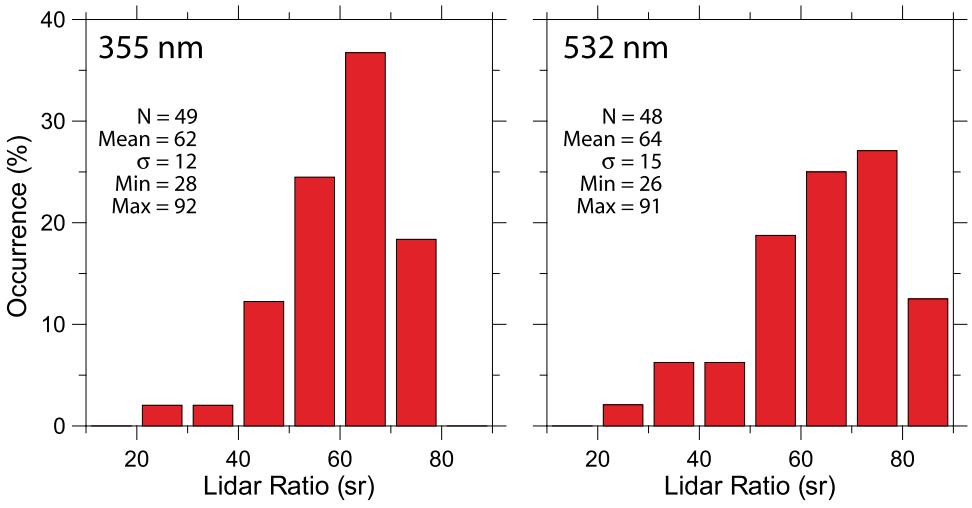

Figure 16. Frequency distributions of the layer mean lidar ratio at (left) 355 and (right) 532 nm. Lidar ratios for the layer from 1500–2500 m height are considered. Statistics are based on *N* observations. Mean values, standard deviations, maximum and minimum values are given as numbers.

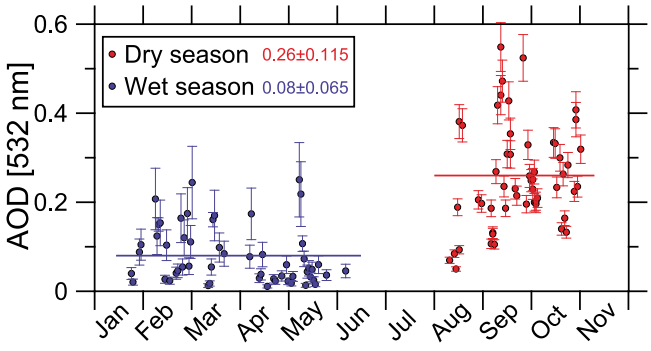

Figure 17. Time series of the 532 nm AOD during the wet season (blue) and the dry season (red) in 2008. Horizontal lines indicate the AOD means (given also as numbers). Horizontal lines indicate the mean values (given also as numbers).

[60] A unique feature of biomass burning aerosol is also the wide spread of lidar-ratio values, here from 25–95 sr, as mentioned above. This reflects the influence of particle aging, including cloud processing of the particles, and differences in the burning material and fire type.

4.3.4. Aerosol Optical Depth

[61] The time series of the 532 nm AOD measured with the Polly^{XT} lidar from 22 January to 11 November 2008 is shown in Figure 17. Pristine, clean background conditions with AOD < 0.05 were often interrupted (on an almost regular basis) by advection of African aerosols causing AOD values >0.05. The cleanest conditions were most frequently found in April and May 2008 because of the decreasing fire activity at the end of western African fire season. The AOD values did not exceed 0.25 during the entire wet season 2008. The mean wet-season AOD was found to be 0.08 and was thus about three times smaller than the one for the dry season. However, under pristine background conditions a mean AOD as low as 0.03 was observed whereas an average value of 0.14 was found during periods with African aerosol.

[62] In the dry season, a high AOD variability was observed. AOD values ranged from 0.05–0.55. The highest AOD values were observed in September and October, when the fire activity east and thus upwind of the lidar site was highest.

[63] The observed inter-seasonal and in-season behavior of the lidar-derived optical aerosol properties is in good agreement with findings from measurements of optical aerosol properties in Alta Floresta, Rondônia, in southern Amazonia [*Guyon et al.*, 2003]. A high day-to-day variability during the dry season was observed as well as a strong contrast between the wet and the dry season in southern Amazonia. However, the magnitude of the observed variations in the optical aerosol properties was much lower at the lidar site. The area north of Manaus is obviously less affected by smoke pollution than regions in southern Amazonia.

[64] The frequency distributions of the lidar-derived AOD (532 nm) for the wet and dry season are shown in Figure 18. Again, a strong contrast between the wet and dry season is visible. Almost 50% out of all wet season observations yield AODs < 0.05, whereas 50% out of the dry season cases showed AODs > 0.25 at 532 nm.

[65] The ratio of AOD_{ML} of the mixing layer to the total AOD for the dry season is shown in Figure 19 and indicates that the mixing layer height can not be regarded as a barrier for vertical aerosol exchange. In only 25% out of all cases the AOD is controlled by aerosols in the mixing layer. These

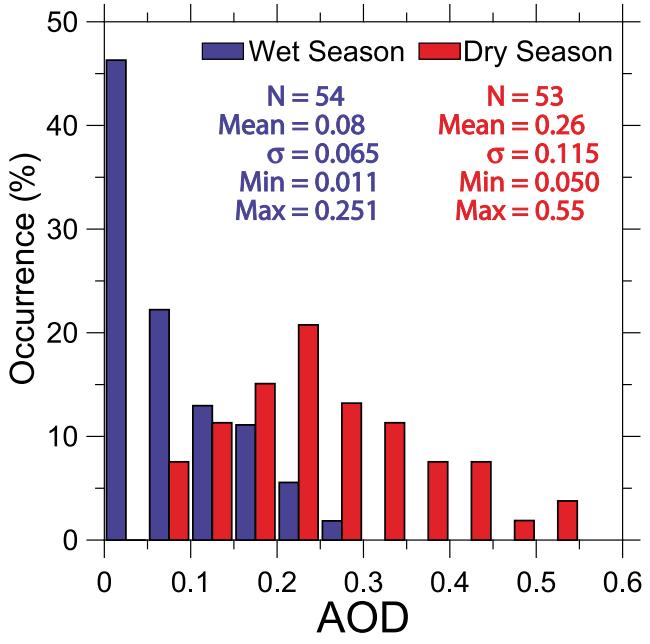

Figure 18. Frequency distribution of the lidar-derived 532 nm AOD for the wet (blue) and dry (red) season 2008. *N* observations were analyzed. Mean values, standard deviations, maximum and minimum values are given as numbers.

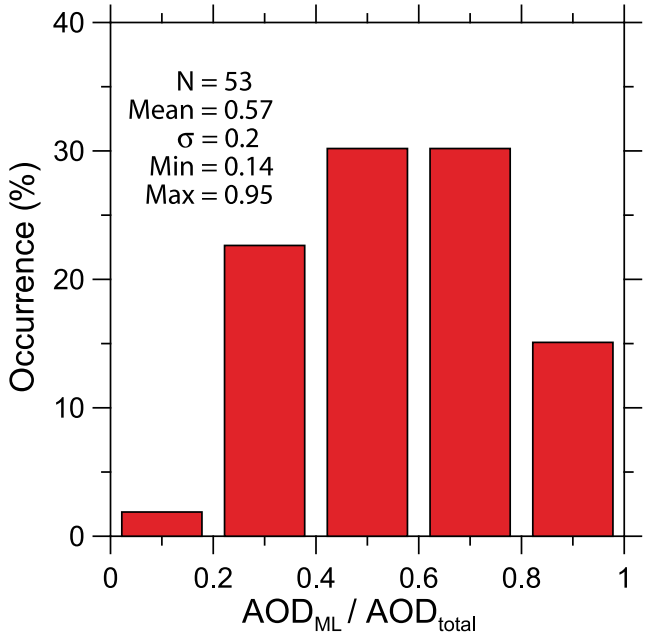

Figure 19. Frequency distribution of the AOD fraction that is contributed by the mixing layer (with top usually below 1500 m height) to the total tropospheric AOD for the dry season 2008. *N* observations were analyzed. Mean values, standard deviations, maximum and minimum values are given as numbers.

Table 2. Monthly Mean AOD at 532 nm Derived From Lidar Observations in 2008 and From AERONET Observations in the Northern Forest Region for the 1999–2006 Period as Published by *Schafer et al.* [2008][a]

	Jan	Feb	Mar	Apr	May	Jun	Jul	Aug	Sep	Oct	Nov	Dec
Lidar 2008	0.06	0.10	0.09	0.05	0.07	–	–	0.18	0.29	0.25	–	–
AERONET	0.14	0.11	0.12	0.09	0.10	0.08	0.10	0.18	0.26	0.37	0.36	0.33

[a]The AERONET AODs were converted from 440 nm to 532 nm by using the published monthly mean Ångström exponents.

findings corroborate results from airborne measurements during the dry season in Rondônia [*Guyon et al.*, 2005]. No differences in the aerosol characteristics within and above the mixing layer were found during these research flights. Our findings also agree well with airborne lidar observations by *Browell et al.* [1988] drawn from 11 flights in northern Brazil near the Amazon river in the summer of 1985. It was found that significant amounts of aerosol were above the mixing layer. The vertical distribution was generally very inhomogeneous.

[66] *Schafer et al.* [2008] analyzed several years of AERONET observations at 15 sites in Amazonia between 1999 and 2006. Monthly mean AOD values at 440 nm were presented for the cerrado region, southern forest region, and the northern forest regions (the region of the EUCAARI lidar site). A comparison of monthly mean 532 nm AOD values determined with lidar and obtained from the AERONET photometers in northern Amazonia (4 stations, one close to the lidar site, 3 far more east) is shown in Table 2. A good agreement is found for the dry season.

[67] For the wet season, *Schafer et al.* [2008] reported AOD values between 0.1 and 0.14 (532 nm) in the northern forest region. This is much higher than observed with the lidar (0.05–0.1 at 532 nm). A stronger influence of African aerosol transport on the stations east of the lidar site may have caused this result as well as generally increased aerosol transport from Africa toward Amazonia between 1999 and 2006.

[68] Finally, a summarizing overview of the lidar observations during the wet and dry season 2008 is presented in Table 3. Mean values and respective standard deviations for the aerosol properties discussed before are given.

5. Summary

[69] For the first time the aerosol conditions over the Amazon Basin were continuously monitored in terms of height profiles of particle optical and microphysical properties over almost one year. An automated, advanced Raman lidar was used that permits aerosol profiling at natural environmental conditions, i.e., at ambient humidity conditions (without any manipulation of the aerosol to be measured as is needed in the case of in situ sampling).

[70] One of the key issues was to contrast the aerosol conditions during the wet season and during the highly polluted dry season. It was found that pristine environmental conditions occurring during the wet season were frequently interrupted by advection of African smoke and dust plumes. During these events, particle extinction coefficients and optical depths were observed to be enhanced by a factor of 4 (on average).

[71] In the dry season, the backscatter, extinction, and optical depth values were, on average, increased by a factor of 6 in the main biomass burning layers at heights <2 km (compared to the pristine wet season aerosol conditions).

[72] Based on two cases studies it was shown that the optical properties of the biomass burning aerosol can be rather different as a result of the burning type, burning material, transport times, aging processes, and other effects. The findings confirm previous studies.

[73] The statistical analysis of the complete lidar data set revealed also strong differences between the pristine wet and the polluted dry season. Under pristine conditions, the particle extinction coefficients at 532 nm wavelength were frequently as low as 10–30 Mm^{-1}, the particle optical depth was <0.05, and aerosol was trapped in the lowermost 2.5 km of the troposphere. During the dry season, the biomass burning smoke plumes reached to 3–5 km height. The AOD scale height was however usually below 2 km height. On average, particle extinction coefficients at 532 nm wavelength were of the order of 100 Mm^{-1} in the main pollution layer (up to 2 km height) and 30–50 Mm^{-1} from 2–4 km height. Ångström exponents were mainly between 1.0 and 1.5, and lidar ratios accumulated from 50–80 sr. On average during the wet season 2008, the AOD at 532 nm was 0.03 under background conditions and 0.14 during periods of African aerosol intrusion. A mean AOD of 0.26 was found during the dry season 2008.

[74] As already demonstrated in many aerosol lidar studies, the lidar ratios (especially when measured at two wavelengths) and the backscatter- and extinction-related Ångström exponents provide a solid basis for aerosol typing. Depolarization ratio observations are in addition of value in areas close to deserts or in outflow regimes of desert dust.

Table 3. Mean Values and Standard Deviations of Lidar-Derived Particle Optical Properties and Layer Height Parameter[a]

Quantity	Dry Season	Wet Season
	Tropospheric Column	
AOD (355 nm)	0.38 ± 0.18	0.13 ± 0.06
AOD (532 nm)	0.26 ± 0.12	0.08 ± 0.07
AL top	4.1 ± 0.8 km	2.5 ± 0.5 km
H_{aer}	1.6 ± 0.3 km	1.2 ± 0.3 km
H_{AOD95}	3.0 ± 0.5 km	2.3 ± 0.6 km
ML top	1.5 ± 0.4 km	1.1 ± 0.3 km
	Mixing Layer	
β (355 nm)	2.63 ± 0.99 Mm^{-1} sr^{-1}	1.18 ± 0.52 Mm^{-1} sr^{-1}
β (532 nm)	1.44 ± 0.69 Mm^{-1} sr^{-1}	0.62 ± 0.50 Mm^{-1} sr^{-1}
β (1064 nm)	0.50 ± 0.21 Mm^{-1} sr^{-1}	0.24 ± 0.26 Mm^{-1} sr^{-1}
	1500–2500 m Height Range	
α (355 nm)	118 ± 64 Mm^{-1}	-
α (532 nm)	70 ± 38 Mm^{-1}	-
β (355 nm)	1.83 ± 1.15 Mm^{-1} sr^{-1}	0.41 ± 0.33 Mm^{-1} sr^{-1}
β (532 nm)	1.09 ± 0.67 Mm^{-1} sr^{-1}	0.30 ± 0.35 Mm^{-1} sr^{-1}
β (1064 nm)	0.48 ± 0.20 Mm^{-1} sr^{-1}	0.13 ± 0.18 Mm^{-1} sr^{-1}
Lidar ratio (355 nm)	62 ± 12 sr	-
Lidar ratio (532 nm)	64 ± 15 sr	-
$a_{\alpha 355/532}$	1.17 ± 0.44	-
$a_{\beta 355/532}$	1.27 ± 0.34	1.22 ± 0.59
$a_{\beta 532/1064}$	1.16 ± 0.27	1.19 ± 0.36

[a]Values are presented for the tropospheric column, for the mixing layer, and the central part of the smoke plumes (1500–2500 m height range). Particle backscatter coefficient, extinction coefficient, Ångström exponent, and particle optical depth are denoted as β, α, å, and AOD, respectively.

The present study adds a new important data set to the lidar-based global aerosol climatology. The study is simultaneously another example how powerful nowadays aerosol lidars can contribute to atmospheric science related to atmospheric composition and climate change. With automated lidar systems this research can be done at even rather inconvenient places like tropical forest (high humidity, high concentration of insects that affect the optics and the overall performance of the lidar).

[75] **Acknowledgments.** We thank the National Institute for Amazonia Research (INPA) and the AMAZE-08 team, especially Scot Martin, for their support. EUCAARI was funded by the European Union (FP7, grant 036833-2). Paulo Artaxo acknowledges CNPq and FAPESP Thematic Project AEROCLIMA 2008/58100-2. This project was also funded by the EU FP6 project EUCAARI (contract 34684). Some analyses and visualizations used in this paper were produced with the Giovanni online data system, developed and maintained by the NASA GES DISC. We also acknowledge the MODIS mission scientists and associated NASA personnel for the production of the data used in this research effort. We thank Mika Komppula for providing ECMWF data.

References

Althausen, D., R. Engelmann, H. Baars, B. Heese, A. Ansmann, D. Müller, and M. Komppula (2009), Portable Raman lidar PollyXT for automated profiling of aerosol backscatter, extinction, and depolarization, *J. Atmos. Oceanic Technol.*, *26*, 2366–2378, doi:10.1175/2009JTECHA1304.1.

Andreae, M. O., D. Rosenfeld, P. Artaxo, A. A. Costa, G. P. Frank, K. M. Longo, and M. A. F. Silva-Dias (2004), Smoking rain clouds over the Amazon, *Science*, *303*, 1337–1342.

Ansmann, A., and D. Müller (2005), Lidar and atmospheric aerosol particles, in *Lidar—Range-Resolved Optical Remote Sensing of the Atmosphere*, *Springer Ser. Opt. Sci.*, vol. 102, edited by C. Weitkamp, pp. 105–141, Springer, Berlin.

Ansmann, A., U. Wandinger, M. Riebesell, C. Weitkamp, and W. Michaelis (1992), Independent measurement of extinction and backscatter profiles in cirrus clouds by using a combined Raman elastic-backscatter lidar, *Appl. Opt.*, *31*, 7113–7131, doi:10.1364/AO.31.007113.

Ansmann, A., H. Baars, M. Tesche, D. Müller, D. Althausen, R. Engelmann, T. Pauliquevis, and P. Artaxo (2009), Dust and smoke transport from Africa to South America: Lidar profiling over Cape Verde and the Amazon rainforest, *Geophys. Res. Lett.*, *36*, L11802, doi:10.1029/2009GL037923.

Ansmann, A., P. Seifert, M. Tesche, and U. Wandinger (2012), Profiling of fine and coarse particle mass: Case studies of Saharan dust and Eyjafjallajökull/Grimsvötn volcanic plumes, *Atmos. Chem. Phys. Discuss.*, *12*(5), 13,363–13,403, doi:10.5194/acpd-12-13363-2012.

Artaxo, P., H. Storms, F. Bruynseels, R. van Grieken, and W. Maenhaut (1988), Composition and sources of aerosols from the Amazon Basin, *J. Geophys. Res.*, *93*, 1605–1615, doi:10.1029/JD093iD02p01605.

Artaxo, P., W. Maenhaut, H. Stroms, and R. van Grieken (1990), Aerosol characteristics and sources for the Amazon Basin during the wet season, *J. Geophys. Res.*, *95*, 16,971–16,985, doi:10.1029/JD095iD10p16971.

Artaxo, P., F. Gerab, M. Yamasoe, and J. Martins (1994), Fine mode aerosol composition at three long-term atmospheric monitoring sites in the Amazon Basin, *J. Geophys. Res.*, *99*, 22,857–22,868.

Artaxo, P., J. V. Martins, M. A. Yamasoe, A. S. Procopio, T. M. Pauliquevis, M. O. Andreae, P. Guyon, L. V. Gatti, and A. M. C. Leal (2002), Physical and chemical properties of aerosols in the wet and dry seasons in Rondônia, Amazonia, *J. Geophys. Res.*, *107*(D20), 8081, doi:10.1029/2001JD000666.

Baars, H., A. Ansmann, D. Althausen, R. Engelmann, P. Artaxo, T. Pauliquevis, and R. Souza (2011), Further evidence for significant smoke transport from Africa to Amazonia, *Geophys. Res. Lett.*, *38*, L20802, doi:10.1029/2011GL049200.

Ben-Ami, Y., I. Koren, Y. Rudich, P. Artaxo, S. T. Martin, and M. O. Andreae (2010), Transport of North African dust from the Bodélé depression to the Amazon Basin: A case study, *Atmos. Chem. Phys.*, *10*, 7533–7544, doi:10.5194/acp-10-7533-2010.

Browell, E. V., G. L. Gregory, R. C. Harriss, and V. W. J. H. Kirchhoff (1988), Tropospheric ozone and aerosol distributions across the Amazon Basin, *J. Geophys. Res.*, *93*, 1431–1451, doi:10.1029/JD093iD02p01431.

Bucholtz, A. (1995), Rayleigh-scattering calculations for the terrestrial atmosphere, *Appl. Opt.*, *34*, 2765–2773.

Chand, D., P. Guyon, P. Artaxo, O. Schmid, G. P. Frank, L. V. Rizzo, O. L. Mayol-Bracero, L. V. Gatti, and M. O. Andreae (2006), Optical and physical properties of aerosols in the boundary layer and free troposphere over the Amazon Basin during the biomass burning season, *Atmos. Chem. Phys.*, *6*, 2911–2925.

Damoah, R., N. Spichtinger, C. Forster, P. James, I. Mattis, U. Wandinger, S. Beirle, T. Wagner, and A. Stohl (2004), Around the world in 17 days—Hemispheric-scale transport of forest fire smoke from Russia in May 2003, *Atmos. Chem. Phys.*, *4*, 1311–1321.

Draxler, R. R., and G. D. Hess (1998), An overview of the HYSPLIT4 modelling system for trajectories, dispersion, and deposition, *Aust. Meteorol. Mag.*, *47*, 295–308.

Draxler, R. R., B. Stunder, G. D. Rolph, A. Stein, and A. Taylor (2009), HYSPLIT4 user's guide, report, NOAA Air Resour. Lab., Silver Spring, Md. [Available at http://www.arl.noaa.gov/ready/hysplit4.html.]

Dubovik, O., B. Holben, T. F. Eck, A. Smirnov, Y. J. Kaufman, M. D. King, D. Tanré, and I. Slutsker (2002), Variability of absorption and optical properties of key aerosol types observed in worldwide locations, *J. Atmos. Sci.*, *59*, 590–608, doi:10.1175/1520-0469(2002)059.

Fernald, F. G. (1984), Analysis of atmospheric lidar observations: Some comments, *Appl. Opt.*, *23*, 652–653.

Formenti, P., M. O. Andreae, L. Lange, G. Roberts, J. Cafmeyer, I. Rajta, W. Maenhaut, B. N. Holben, P. Artaxo, and J. Lelieveld (2001), Saharan dust in Brazil and Suriname during the Large-Scale Biosphere-Atmosphere Experiment in Amazonia (LBA)—Cooperative LBA Regional Experiment (CLAIRE) in March 1998, *J. Geophys. Res.*, *106*, 14,919–14,934, doi:10.1029/2000JD900827.

Franke, K., A. Ansmann, D. Müller, D. Althausen, C. Venkataraman, M. S. Reddy, F. Wagner, and R. Scheele (2003), Optical properties of the Indo-Asian haze layer over the tropical Indian Ocean, *J. Geophys. Res.*, *108*(D2), 4059, doi:10.1029/2002JD002473.

Giglio, L., J. Descloitres, C. O. Justice, and Y. J. Kaufman (2003), An enhanced contextual fire detection algorithm for MODIS, *Remote Sens. Environ.*, *87*, 273–282, doi:10.1016/S0034-4257(03)00184-6.

Guyon, P., B. Graham, J. Beck, O. Boucher, E. Gerasopoulos, O. L. Mayol-Bracero, G. C. Roberts, P. Artaxo, and M. O. Andreae (2003), Physical properties and concentration of aerosol particles over the Amazon tropical forest during background and biomass burning conditions, *Atmos. Chem. Phys.*, *3*, 951–967.

Guyon, P., et al. (2005), Airborne measurements of trace gas and aerosol particle emissions from biomass burning in Amazonia, *Atmos. Chem. Phys.*, *5*, 2989–3002.

Hänel, A., H. Baars, D. Althausen, A. Ansmann, R. Engelmann, and J. Y. Sun (2012), One-year aerosol profiling with EUCAARI Raman lidar at Shangdianzi GAW station: Beijing plume and seasonal variations, *J. Geophys. Res.*, *117*, D13201, doi:10.1029/2012JD017577.

Holben, B. N., A. Setzer, T. F. Eck, A. Pereira, and I. Slutsker (1996), Effect of dry-season biomass burning on Amazon basin aerosol concentrations and optical properties, 1992–1994, *J. Geophys. Res.*, *101*, 19,465–19,482, doi:10.1029/96JD01114.

Holben, B. N., et al. (2001), An emerging ground-based aerosol climatology: Aerosol optical depth from AERONET, *J. Geophys. Res.*, *106*, 12,067–12,098, doi:10.1029/2001JD900014.

Kaufman, Y. J., A. Setzer, D. Ward, D. Tanré, B. N. Holben, P. Menzel, M. C. Pereira, and R. Rasmussen (1992), Biomass Burning Airborne and Spaceborne Experiment in the Amazonas (BASE-A), *J. Geophys. Res.*, *97*, 14,581–14,599, doi:10.1029/92JD00275.

Kaufman, Y. J., et al. (1998), Smoke, Clouds, and Radiation-Brazil (SCAR-B) experiment, *J. Geophys. Res.*, *103*, 31,783–31,808, doi:10.1029/98JD02281.

Kaufman, Y. J., I. Koren, L. A. Remer, D. Tanré, P. Ginoux, and S. Fan (2005), Dust transport and deposition observed from the Terra-Moderate Resolution Imaging Spectroradiometer (MODIS) spacecraft over the Atlantic Ocean, *J. Geophys. Res.*, *110*, D10S12, doi:10.1029/2003JD004436.

Komppula, M., et al. (2012), Technical note: One year of Raman-lidar measurements in Gual Pahari EUCAARI site close to New Delhi in India—Seasonal characteristics of the aerosol vertical structure, *Atmos. Chem. Phys.*, *12*(10), 4513–4524, doi:10.5194/acp-12-4513-2012.

Koren, I., Y. J. Kaufman, L. A. Remer, and J. V. Martins (2004), Measurement of the effect of Amazon smoke on inhibition of cloud formation, *Science*, *303*, 1342–1345, doi:10.1126/science.1089424.

Kuhn, U., et al. (2010), Impact of Manaus City on the Amazon Green Ocean atmosphere: Ozone production, precursor sensitivity and aerosol load, *Atmos. Chem. Phys.*, *10*, 9251–9282, doi:10.5194/acp-10-9251-2010.

Kulmala, M., et al. (2011), General overview: European Integrated project on Aerosol Cloud Climate and Air Quality interactions (EUCAARI): Integrating aerosol research from nano to global scales, *Atmos. Chem. Phys.*, *11*(24), 13,061–13,143, doi:10.5194/acp-11-13061-2011.

Martin, S. T., et al. (2010a), Sources and properties of Amazonian aerosol particles, *Rev. Geophys.*, *48*, RG2002, doi:10.1029/2008RG000280.

Martin, S. T., et al. (2010b), An overview of the Amazonian Aerosol Characterization Experiment 2008 (AMAZE-08), *Atmos. Chem. Phys.*, *10*, 11,415–11,438, doi:10.5194/acp-10-11415-2010.

Mattis, I., A. Ansmann, U. Wandinger, and D. Müller (2003), Unexpectedly high aerosol load in the free troposphere over central Europe in spring/summer 2003, *Geophys. Res. Lett.*, *30*(22), 2178, doi:10.1029/2003GL018442.

Müller, D., U. Wandinger, and A. Ansmann (1999a), Microphysical particle parameters from extinction and backscatter lidar data by inversion with regularization: Simulation, *Appl. Opt.*, *38*, 2358–2368, doi:10.1364/AO.38.002358.

Müller, D., U. Wandinger, and A. Ansmann (1999b), Microphysical particle parameters from extinction and backscatter lidar data by inversion with regularization: Theory, *Appl. Opt.*, *38*, 2346–2357, doi:10.1364/AO.38.002346.

Müller, D., F. Wagner, U. Wandinger, A. Ansmann, M. Wendisch, D. Althausen, and W. von Hoyningen-Huene (2000), Microphysical particle parameters from extinction and backscatter lidar data by inversion with regularization: Experiment, *Appl. Opt.*, *39*, 1879–1892, doi:10.1364/AO.39.001879.

Müller, D., I. Mattis, U. Wandinger, A. Ansmann, D. Althausen, and A. Stohl (2005), Raman lidar observations of aged Siberian and Canadian forest fire smoke in the free troposphere over Germany in 2003: Microphysical particle characterization, *J. Geophys. Res.*, *110*, D17201, doi:10.1029/2004JD005756.

Müller, D., I. Mattis, A. Ansmann, U. Wandinger, C. Ritter, and D. Kaiser (2007a), Multiwavelength Raman lidar observations of particle growth during long-range transport of forest-fire smoke in the free troposphere, *Geophys. Res. Lett.*, *34*, L05803, doi:10.1029/2006GL027936.

Müller, D., A. Ansmann, I. Mattis, M. Tesche, U. Wandinger, D. Althausen, and G. Pisani (2007b), Aerosol-type-dependent lidar ratios observed with Raman lidar, *J. Geophys. Res.*, *112*, D16202, doi:10.1029/2006JD008292.

Murayama, T., H. Okamoto, N. Kaneyasu, H. Kamataki, and K. Miura (1999), Application of lidar depolarization measurement in the atmospheric boundary layer: Effects of dust and sea-salt particles, *J. Geophys. Res.*, *104*, 31,781–31,792, doi:10.1029/1999JD900503.

Nobre, C. A., M. A. Silva Dias, A. Culf, J. Polcher, J. H. C. Gash, J. Marengo, and R. Avissar (2004), The Amazonian climate, in *Vegetation, Water, Humans and the Climate: A New Perspective on an Interactive System*, edited by P. Kabat, pp. 79–92, Springer, Berlin.

O'Neill, N. T., T. F. Eck, B. N. Holben, A. Smirnov, A. Royer, and Z. Li (2002), Optical properties of boreal forest fire smoke derived from Sun photometry, *J. Geophys. Res.*, *107*(D11), 4125, doi:10.1029/2001JD000877.

Pappalardo, G., et al. (2010), EARLINET correlative measurements for CALIPSO: First intercomparison results, *J. Geophys. Res.*, *115*, D00H19, doi:10.1029/2009JD012147.

Pöschl, U., et al. (2010), Rainforest aerosols as biogenic nuclei of clouds and precipitation in the Amazon, *Science*, *329*, 1513–1516, doi:10.1126/science.1191056.

Reid, J. S., and P. V. Hobbs (1998), Physical and optical properties of young smoke from individual biomass fires in Brazil, *J. Geophys. Res.*, *103*, 32,013–32,030, doi:10.1029/98JD00159.

Reid, J. S., P. V. Hobbs, R. J. Ferek, D. R. Blake, J. V. Martins, M. R. Dunlap, and C. Liousse (1998), Physical, chemical, and optical properties of regional hazes dominated by smoke in Brazil, *J. Geophys. Res.*, *103*, 32,059–32,080, doi:10.1029/98JD00458.

Reid, J. S., P. V. Hobbs, A. L. Rangno, and D. A. Hegg (1999), Relationships between cloud droplet effective radius, liquid water content, and droplet concentration for warm clouds in Brazil embedded in biomass smoke, *J. Geophys. Res.*, *104*, 6145–6154, doi:10.1029/1998JD200119.

Reid, J. S., R. Koppmann, T. F. Eck, and D. P. Eleuterio (2005), A review of biomass burning emissions part II: Intensive physical properties of biomass burning particles, *Atmos. Chem. Phys.*, *5*(3), 799–825, doi:10.5194/acp-5-799-2005.

Remer, L. A., et al. (2005), The MODIS aerosol algorithm, products, and validation, *J. Atmos. Sci.*, *62*, 947–973, doi:10.1175/JAS3385.1.

Rissler, J., E. Swietlicki, J. Zhou, G. Roberts, M. O. Andreae, L. V. Gatti, and P. Artaxo (2004), Physical properties of the sub-micrometer aerosol over the Amazon rain forest during the wet-to-dry season transition—Comparison of modeled and measured CCN concentrations, *Atmos. Chem. Phys.*, *4*, 2119–2143, doi:10.5194/acp-4-2119-2004.

Rissler, J., A. Vestin, E. Swietlicki, G. Fisch, J. Zhou, P. Artaxo, and M. O. Andreae (2006), Size distribution and hygroscopic properties of aerosol particles from dry-season biomass burning in Amazonia, *Atmos. Chem. Phys.*, *6*, 471–491.

Roberts, G. C., M. O. Andreae, J. Zhou, and P. Artaxo (2001), Cloud condensation nuclei in the Amazon Basin: "Marine" conditions over a continent?, *Geophys. Res. Lett.*, *28*, 2807–2810, doi:10.1029/2000GL012585.

Rosenfeld, D., U. Lohmann, G. B. Raga, C. D. O'Dowd, M. Kulmala, S. Fuzzi, A. Reissell, and M. O. Andreae (2008), Flood or drought: How do aerosols affect precipitation?, *Science*, *321*, 1309–1313, doi:10.1126/science.1160606.

Ross, J. L., P. V. Hobbs, and B. Holben (1998), Radiative characteristics of regional hazes dominated by smoke from biomass burning in Brazil: Closure tests and direct radiative forcing, *J. Geophys. Res.*, *103*, 31,925–31,942.

Schafer, J. S., T. F. Eck, B. N. Holben, P. Artaxo, and A. F. Duarte (2008), Characterization of the optical properties of atmospheric aerosols in Amazônia from long-term AERONET monitoring (1993–1995 and 1999–2006), *J. Geophys. Res.*, *113*, D04204, doi:10.1029/2007JD009319.

Smirnov, A., et al. (2009), Maritime Aerosol Network as a component of Aerosol Robotic Network, *J. Geophys. Res.*, *114*, D06204, doi:10.1029/2008JD011257.

Swap, R., M. Garstang, S. Greco, R. Talbot, and P. Kållberg (1992), Saharan dust in the Amazon Basin, *Tellus, Ser. B*, *44*, 133–149, doi:10.1034/j.1600-0889.1992.t01-1-00005.x.

Talbot, R. W., M. O. Andreae, H. Berresheim, P. Artaxo, M. Garstang, R. C. Harriss, and K. M. Beecher (1990), Aerosol chemistry during the wet season in Central Amazonia: The influence of long-range transport, *J. Geophys. Res.*, *95*, 16,955–16,969, doi:10.1029/JD095iD10p16955.

Tesche, M., D. Müller, S. Groß, A. Ansmann, D. Althausen, V. Freudenthaler, B. Weinzierl, A. Veira, and Petzold (2011), Optical and microphysical properties of smoke over Cape Verde inferred from multiwavelength lidar measurements, *Tellus, Ser. B*, *63*, 677–694, doi:10.1111/j.1600-0889.2011.00549.x.

Wandinger, U., and A. Ansmann (2002), Experimental determination of the lidar overlap profile with Raman lidar, *Appl. Opt.*, *41*, 511–514.

Ward, D. E., R. A. Susott, J. B. Kauffman, R. E. Babbitt, D. L. Cummings, B. Dias, B. N. Holden, Y. J. Kaufman, R. A. Rasmussen, and A. W. Setzer (1992), Smoke and fire characteristics for Cerrado and deforestation burns in Brazil: BASE-B experiment, *J. Geophys. Res.*, *97*, 14,601–14,619.

Wilson, S. R., and B. W. Forgan (2002), Aerosol optical depth at Cape Grim, Tasmania, 1986–1999, *J. Geophys. Res.*, *107*(D8), 4068, doi:10.1029/2001JD000398.

Zhou, J., E. Swietlicki, H. C. Hansson, and P. Artaxo (2002), Submicrometer aerosol particle size distribution and hygroscopic growth measured in the Amazon rain forest during the wet season, *J. Geophys. Res.*, *107*(D20), 8055, doi:10.1029/2000JD000203.